J|A|C|S
ARTICLES
Published on Web 08/05/2006

How Does Single Oxygen Atom Addition Affect the Properties of an Fe−Nitrile Hydratase Analogue? The Compensatory Role of the Unmodified Thiolate

Priscilla Lugo-Mas,[†] Abhishek Dey,[‡] Liang Xu,[†] Steven D. Davin,[†] Jason Benedict,[†] Werner Kaminsky,[†,#] Keith O. Hodgson,[*,‡,§] Britt Hedman,[*,§] Edward I. Solomon,[*,‡] and Julie A. Kovacs[*,†]

Contribution from the Department of Chemistry, University of Washington, Box 351700, Seattle, Washington 98195-1700, Department of Chemistry, Stanford University, Stanford, California 94305, and Stanford Synchrotron Radiation Laboratory, SLAC, Stanford University, Menlo Park, California 94025

Received April 18, 2006; E-mail: kovacs@chem.washington.edu

Abstract: Nitrile hydratase (NHase) is one of a growing number of enzymes shown to contain post-translationally modified cysteine sulfenic acids (Cys-SOH). Cysteine sulfenic acids have been shown to play diverse roles in cellular processes, including transcriptional regulation, signal transduction, and the regulation of oxygen metabolism and oxidative stress responses. The function of the cysteine sulfenic acid coordinated to the iron active site of NHase is unknown. Herein we report the first example of a sulfenate-ligated iron complex, $[Fe^{III}(ADIT)(ADIT\text{-}O)]^+$ (**5**), and compare its electronic and magnetic properties with those of structurally related complexes in which the sulfur oxidation state and protonation state have been systematically altered. Oxygen atom addition was found to decrease the unmodified thiolate Fe−S bond length and blue-shift the ligand-to-metal charge-transfer band (without loss of intensity). S K-edge X-ray absorption spectroscopy and density functional theory calculations show that, although the modified RS-O^- fragment is incapable of forming a π bond with the Fe^{III} center, the unmodified thiolate compensates for this loss of π bonding by increasing its covalent bond strength. The redox potential shifts only slightly (75 mV), and the magnetic properties are not affected (the $S = {}^1/_2$ spin state is maintained). The coordinated sulfenate S−O bond is activated and fairly polarized (S^+-O^-). Addition of strong acids at low temperatures results in the reversible protonation of sulfenate-ligated **5**. An X-ray structure demonstrates that Zn^{2+} binds to the sulfenate oxygen to afford $[Fe^{III}(ADIT)(ADIT\text{-}O\text{-}ZnCl_3)]$ (**6**). The coordination of $ZnCl_3^-$ to the RS-O^- unit causes the covalent overlap with the unmodified thiolate to increase further. A possible catalytic role for the unmodified NHase thiolate, involving its ability to "tune" the electronics in response to protonation of the sulfenate (RS-O^-) oxygen and/or substrate binding, is discussed.

Nitrile hydratases (NHases) are non-heme iron enzymes that convert nitriles to less toxic amides cleanly, and rapidly, under mild conditions.[1−16] It is unusual for a hydrolytic metalloenzyme to incorporate iron, as opposed to zinc,[17,18] presumably because, unlike other metal ions, Zn^{2+} is not complicated by redox chemistry. Iron, on the other hand, can promote unwanted side reactions with dioxygen (i.e., Fenton chemistry involving $OH^\bullet$ radicals) upon reduction to the Fe^{2+} oxidation state.[19,20] The

[†] University of Washington.
[‡] Stanford University.
[§] Stanford Synchrotron Radiation Laboratory.
[#] University of Washington staff crystallographer.

(1) Nojiri, M.; Yohda, M.; Odaka, M.; Matsushita, Y.; Tsujimura, M.; Yoshida, T.; Dohmae, N.; Takio, K.; Endo, I. *J. Biochem.* **1999**, *125*, 696−704.
(2) Noguchi, T.; Hoshino, M.; Tsujimura, M.; Odaka, M.; Inoue, Y.; Endo, I. *Biochemistry* **1996**, *35*, 16777−16781.
(3) Nagashima, S.; Nakasako, M.; Naoshi, D.; Tsujimura, M.; Takio, K.; Odaka, M.; Yohda, M.; Kamiya, N.; Endo, I. *Nat. Struct. Biol.* **1998**, *5*, 347−351.
(4) Odaka, M.; Fujii, K.; Hoshino, M.; Noguchi, T.; Tsujimura, M.; Nagashima, S.; Yohada, N.; Nagamune, T.; Inoue, I.; Endo, I. *J. Am. Chem. Soc.* **1997**, *119*, 3785−3791.
(5) Nagasawa, T.; Ryuno, K.; Yamada, H. *Biochem. Biophys. Res. Commun.* **1986**, *139*, 1305−1312.
(6) Odaka, M.; Noguchi, T.; Nagashma, S.; Yohda, M.; Yabuki, S.; Hoshino, M,; Inoue, Y.; Endo, I. *Biochem. Biophys. Res. Commun.* **1996**, *221*, 146−150.
(7) Sugiura, Y.; Kuwahara, J.; Nagasawa, T.; Yamada, H. *J. Am. Chem. Soc.* **1987**, *109*, 5848−5850.
(8) Brennan, B. A.; Jin, H.; Chase, D. B.; Turner, I. M.; Buck, C.; Scarrow, R. C.; Gurbiel, R.; Doan, P.; Hoffman, B. M.; Nelson, M. J. *J. Inorg. Biochem.* **1993**, *51*, 374.
(9) Jin, H.; Turner, I. M., Jr.; Nelson, M. J.; Gurbiel, R. J.; Doan, P. E.; Hoffman, B. M. *J. Am. Chem. Soc.* **1993**, *115*, 5290−5291.
(10) Brennan, B. A.; Alms, G.; Scarrow, R. C. *J. Am. Chem. Soc.* **1996**, *118*, 9194−9195.
(11) Nelson, M. J.; Jin, H.; Turner, I. M., Jr.; Grove, G.; Scarrow, R. C.; Brennan, B. A.; Que, L., Jr. *J. Am. Chem. Soc.* **1991**, *113*, 7072−7073.
(12) Scarrow, R. C.; Brennan, B. A.; Nelson, M. J. *Biochemistry* **1996**, *35*, 10078−10088.
(13) Brennan, B. A.; Cummings, J. G.; Chase, D. B.; Turner, I. M., Jr.; Nelson, M. J. *Biochemistry* **1996**, *35*, 10068−10077.
(14) Yamada, H.; Shimizu, S.; Kobayashi, M. *Chem. Record* **2001**, *1*, 152−161.
(15) Tsujimura, M.; Odaka, M.; Nagashma, S.; Yohda, M.; Endo, I. *J. Biochem.* **1996**, *119*, 407−413.
(16) Nagamune, T.; Honda, J.; Kobayashi, Y.; Sasabe, H.; Endo, I.; Ambe, F. *Hyperfine Interact.* **1992**, *71*, 1271−1274.
(17) Coleman, J. E. *Curr. Opin. Chem. Biol.* **1998**, *2*, 222−234.
(18) Eklund, H.; Branden, C.-I. *Zinc Enzymes*; Wiley: New York, 1983.
(19) Meyerstein, D.; Goldstein, S. *Acc. Chem. Res.* **1999**, *32*, 547−550.
(20) Hlavaty, J. J.; Benner, J. S.; Hornstra, L. J.; Schildkraut, I. *Biochemistry* **2000**, *39*, 3097−3105.

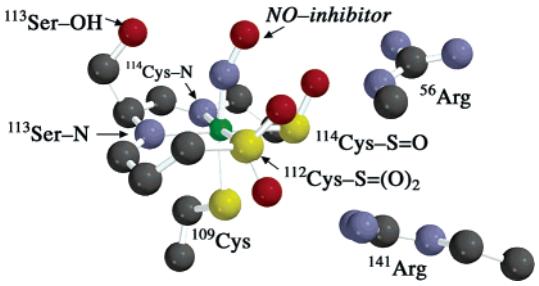

Figure 1. Ball-and-stick diagram of the active site of nitrile hydratase (NHase) drawn using PDB crystallographic coordinates (2AHJ) and Spartan (Wavefunction).

NHase iron site is, however, redox inactive and stabilized in the 3+ oxidation state. The stabilization of Fe^{3+} is accomplished by placing the iron in an electron-rich environment consisting of five anionic ligands—two deprotonated peptide amides and three cysteinates (Figure 1). Two of the three coordinated cysteinate sulfurs are oxidized (post-translationally modified) in NHase — one to a sulfenic acid (^{114}Cys-S-(OH)) and the other to a sulfinate $^{112}CysSO_2^-$.[3,21] The third cysteinate sulfur, which is trans to the inhibitor/substrate binding site and less accessible to solvent, remains unmodified.[3,21−23] ^{34}S-sensitive vibrations, attributed to the doubly and singly oxygenated $\nu_{S=O}$ stretches, are seen in the FT-IR spectra of NHase (from *Rhodococcus* N-771)[24] at 1140, 1030, and 910 cm^{-1}, which shift slightly upon deuteration, providing evidence that at least one of the sulfenate or sulfinate oxygens is either protonated or H-bonded, perhaps to the conserved Arg^{56} and/or Arg^{141} residues. One would expect a metal-bound sulfenate oxygen (RS-(OH)) to be highly acidic. However, sulfur K-edge X-ray absorption spectroscopy (XAS) studies suggest that the sulfenic acid residue is protonated.[25] The sulfinate (RSO_2^-) has been shown to remain unprotonated.[25] The enzyme becomes inactive when a second oxygen atom is added to the sulfenate ^{114}Cys-S-(OH), implying that the singly oxygenated sulfur plays a specific role in catalysis.[26] For this reason, the studies herein focus on the effect of single oxygen atom addition on properties likely to influence catalytic activity. Cysteine sulfenic acids have been shown to play diverse roles in cellular processes, including signal transduction, oxygen metabolism and oxidative stress response, and transcriptional regulation.[27] Catalytically active Cys-SOH are found in NADH peroxidase,[28] NADH oxidase,[29] and peroxyredoxins.[30] Oxygen atom addition to a coordinated thiolate sulfur would be expected to create a more Lewis acidic metal site by withdrawing electron density from the metal ion. Metal ion Lewis acidity would play an important role in the mechanism of nitrile hydrolysis if nitrile binding to the metal ion were involved. The mechanism by which nitriles are hydrolyzed by NHase is unknown, and nitriles are extremely resistant to hydrolysis. However, rates of hydration have been shown to increase dramatically in the presence of a Lewis acidic metal ion capable of coordinating nitriles.

A number of structural models for Fe−NHase and Co−NHase containing oxidized thiolate ligands have been reported,[31−36] and in one case sulfur oxygenation was shown to influence the pK_a of a coordinated water molecule.[37] Very few models containing singly oxygenated sulfurs are available, and none of these contain iron.[38−40] Only one model has been reported containing both a singly oxygenated and a doubly oxygenated thiolate sulfur in the same molecule.[40] The selective incorporation of an odd number of oxygens is nontrivial, since sulfenates (RS-O(H)) are more reactive than thiolates and readily disproportionate to sulfinates (RSO_2^-) and thiolates. Very little is known about how the electronic structure and, more importantly, Fe−S bonding within NHase (or model compounds thereof) respond to oxidation and/or protonation of the coordinated sulfur ligands, and how this might affect reactivity.

Herein, the synthesis and characterization of a series of structurally related Fe−NHase model complexes is described, in which the oxidation and protonation states of one of the thiolates are systematically altered. Comparison of the electronic, magnetic, redox, bonding, and reactivity properties of this series reveals how oxo atom addition and protonation affects the metal ion Lewis acidity. The implications of these findings with respect to how post-translational modification might influence function in NHase will also be discussed. Prior to the work reported herein, there were no examples of sulfenate-ligated iron complexes.

Experimental Section

General Methods. All reactions were performed under an atmosphere of dinitrogen in a glovebox, or using standard Schlenk techniques, or using a custom-made solution cell equipped with a threaded glass connector sized to fit a dip probe. Reagents purchased from commercial vendors were of the highest purity available and used without further purification. Toluene, pentane, Et_2O, and MeCN were rigorously degassed and purified using solvent purification columns housed in a custom stainless steel cabinet, dispensed via a stainless steel Schlenk-line (GlassContour). Methanol (MeOH) and ethanol (EtOH) were distilled from magnesium methoxide or ethoxide. ^{1}H NMR spectra were recorded on Bruker AV 301, Bruker AV 500, or Bruker DRX 499 FT-NMR spectrometers and are referenced to an external standard of tetramethylsilane (TMS) (paramagnetic compounds) or to residual protio-solvent (diamagnetic compounds). EPR spectra were

(21) Murakami, T.; Nojiri, M.; Nakayama, H.; Odaka, M.; Yohda, M.; Dohmae, Na.; Takio, K.; Nagamune, T.; Endo, I. *Protein Sci.* **2000**, *9*, 1024−1030.
(22) Nojiri, M.; Yohda, M.; Odaka, M.; Matsushita, Y.; Tsujimura, M.; Yoshida, T.; Dohmae, N.; Takio, K.; Endo, I. *J. Biochem. (Tokyo)* **1999**, *125*, 696−704.
(23) Tsujimura, M.; Dohmae, N.; Odaka, M.; Chijimatsu, M.; Takio, K.; Yohda, M.; Hoshino, M.; Nagashima, S.; Endo, I. *J. Biol. Chem.* **1997**, *272*, 29454−29459.
(24) Noguchi, T.; Nojiri, M.; Takei, K.; Odaka, M.; Kamiya, N. *Biochemistry* **2003**, *42*, 11642−11650.
(25) Dey, A.; Chow, M.; Taniguchi, K.; Lugo-Mas, P.; Davin, S. D.; Maeda, M.; Kovacs, J. A.; Odaka, M.; Hedman, B.; Hodgson, K. O.; Solomon, E. I. *J. Am. Chem. Soc.* **2006**, *128*, 533−541.
(26) Tsujimura, M.; Odaka, M.; Nakayama, H.; Dohmae, N.; Koshino, H.; Asami, T.; Hoshino, M.; Takio, K.; Yoshida, S.; Maeda, M.; Endo, I. *J. Am. Chem. Soc.* **2003**, *125*, 11532−11538.
(27) Claiborne, A.; Yeh, J. I.; Mallet, C.; Luba, J.; Crane, E. J.; Charrier, V.; Parsonage, D. *Biochemistry* **1999**, *38*, 15407−15416.
(28) Yeh, J. I.; Claiborne, A.; Hol, W. G. I. *Biochemistry* **1996**, *35*, 9951−9957.
(29) Ahmed, S. A.; Claiborne, A. *J. Biol. Chem.* **1989**, *264*, 19864−19870.
(30) Chae, H. Z.; Robison, K.; Poole, L. B.; Church, G.; Storz, G.; Rhee, S. G. *Proc. Natl. Acad. Sci. U.S.A.* **1994**, *91*, 7017−7021.
(31) Mascharak, P. K. *Coord. Chem.* **2002**, *225*, 201−214.
(32) Kobayashi, M.; Shimizu, S. *Eur. J. Biochem.* **1999**, *261*, 1−9.
(33) Boone, A. J.; Chang, C. H.; Greene, S. N.; Herz, T.; Richards, N. G. J. *Coord. Chem. Rev.* **2003**, *238*, 291−314.
(34) Mascharak, P. K.; Harrop, T. C. *Acc. Chem. Res.* **2004**, *37*, 253−260.
(35) Grapperhaus, C. A.; Patra, A. K.; Mashuta, M. S. *Inorg. Chem.* **2002**, *41*, 1039−1041.
(36) Bourles, E.; Alves de Sousa, R.; Galardon, E.; Giorgi, M.; Artaud, I. *Angew. Chem., Int. Ed.* **2005**, *44*, 2−5.
(37) Tyler, L. A.; Noveron, J. C.; Olmstead, M. M.; Mascharak, P. K. *Inorg. Chem.* **2003**, *42*, 5751−5761.
(38) Heinrich, L.; Mary-Verla, A.; Li, Y.; Vaissermann, J.; Chottard, J.-C. *Eur. J. Inorg. Chem.* **2001**, 2203−2206.
(39) Galvez, C.; Ho, D. G.; Azpd, A.; Selke, M. *J. Am. Chem. Soc.* **2001**, *123*, 3381−3382.
(40) Kung, I. Y.; Schweitzer, D.; Shearer, J.; Taylor, W. D.; Jackson, H. L.; Lovell, S.; Kovacs, J. A. *J. Am. Chem. Soc.* **2000**, *122*, 8299−8300.

recorded on a Bruker EPX CW-EPR spectrometer operating at X-band frequency at 7 K. IR spectra were recorded on a Perkin-Elmer 1700 FT-IR spectrometer as KBr pellets. Cyclic voltammograms were recorded in MeCN (100 mM $Bu^n_4N(PF_6)$ solutions) on a PAR 273 potentiostat utilizing a glassy carbon working electrode, a platinum auxiliary electrode, and an SCE reference electrode. Magnetic moments (solution state) were obtained using the Evans' method as modified for superconducting solenoids.[41,42] Temperatures were obtained using Van Geet's method.[43] Solid-state magnetic measurements were obtained with polycrystalline samples in gel-caps using a Quantum Design MPMS S5 SQUID magnetometer. Ambient temperature electronic absorption spectra were recorded on a Hewlett-Packard model 8450 spectrometer, interfaced to an IBM personal computer (PC). Low-temperature electronic absorption spectra were recorded using a Varian Cary 50 spectrophotometer equipped with a fiber optic cable connected to a "dip" ATR probe (C-technologies), with a custom-built two-neck solution sample holder equipped with a threaded glass connector (sized to fit the dip probe). High-temperature electronic absorption spectra were recorded on a Hewlett-Packard model 8453 spectrometer with a Lauda/Brinkmann circulator, model K-2/R, interfaced to an IBM PC. *N*-Sulfonyloxaziridine (**4**)[44] and thiolate-ligated $[Fe^{III}(ADIT)_2]Cl$ (**3**)[45] were synthesized as previously described.

Preparation of $[Fe^{III}(ADIT)(ADIT\text{-}O)](Cl)\cdot MeCN\cdot PhS(O)_2NH_2$ (5a). To a stirred solution of $[Fe^{III}(ADIT)_2]Cl$ (**3**, 0.50 g, 1.2 mmol) in MeOH (20 mL) at −35 °C was added dropwise a pre-cooled (−35 °C) solution of *N*-sulfonyloxaziridine (**4**) (0.43 g, 1.67 mmol) in MeOH (15 mL). The resulting reaction mixture was allowed to stir for 10 min and then stored in a freezer overnight. The volume of the solution was then reduced to dryness under vacuum. The remaining solids were dissolved in MeCN (∼10 mL) and filtered to remove insoluble impurities. The volume of the filtrate was then reduced to ∼2 mL, layered with 20 mL of an Et_2O/pentane solution (2:1), and cooled to −35 °C overnight to afford **5a** (0.32 g, 0.51 mmol, 42%) as a grape-purple crystalline solid. ESI-MS: calcd for $[FeC_{14}H_{30}N_4OS_2]^+$, 390.4; found, 390.3. Electronic absorption, λ_{max} (ϵ): in CH_3CN, 319 (5120), 575 (1690) nm; in MeOH, 319 (3950), 574 (1220) nm; in H_2O, 318 (5450), 572 (1620) nm.

Preparation of Benzenesulfonamide-Free $[Fe^{III}(ADIT)(ADIT\text{-}O)](Cl)\cdot MeCN$ (5b). Addition of 1.0 equiv, as opposed to 1.4 equiv, of *N*-sulfonyloxaziridine (**4**, 0.14 g, 0.55 mmol) to **3** (0.25 g, 0.55 mmol) under the conditions described above afforded, upon crystallization from MeCN/pentane/Et_2O (1:4:6), microcrystalline samples of benzenesulfonamide-free **5b** (0.11 g, 0.24 mmol, 39%) which lacked the $\nu_{S(=O)_2}$ stretches due to cocrystallized benzenesulfonamide in the infrared spectra. IR (KBr pellet), ν (cm^{-1}): 1631 (imine), 931 (S═O) (Figure S-1, Supporting Information). Solution magnetic moment (303 K; MeCN): $\mu_{eff} = 2.33\ \mu_B$. $E_{1/2}$(MeCN) = −945 mV vs SCE. EPR (MeOH/EtOH glass (9:1), 7 K): $g_1 = 2.20$, $g_2 = 2.16$, $g_3 = 1.98$. Anal. Calcd for $FeC_{16}H_{33}ClN_5OS_2$: C, 41.2; H, 7.12; N, 15.0. Found: C, 40.7; H, 6.94; N, 14.5. Sulfenate-ligated **5b** does not appear to react with nitriles (MeCN, isobutyronitrile). Addition of nitriles to **5b** in the presence of H_2O, under basic (pH = 8), acidic (pH = 4.8), and neutral conditions, followed by stirring for 12−72 h at elevated (60 °C), ambient, and low (4 °C) temperatures, resulted in no reaction, as indicated by the absence of hydrolyzed amide or amine products in the ^1H NMR of organics obtained via metal ion removal on a silica gel column.

Preparation of $[Fe^{III}(ADIT)(ADIT\text{-}O\text{-}ZnCl_3)]$ (6). To a stirred solution of **5b** (0.15 g, 0.32 mmol) in CH_3CN (10 mL) at −35 °C was added dropwise a pre-cooled (−35 °C) solution of $ZnCl_2$ (0.08 g, 0.59 mmol) in CH_3CN. The resulting reaction mixture was allowed to stir for 10 min and then stored in a freezer overnight. Filtration of the reaction mixture afforded **7** (0.10 g, 0.18 mmol, 56%) as a midnight-blue crystalline solid. IR (KBr pellet), ν (cm^{-1}): 1624 (imine), 893 (S═O) (Figure S-2, Supporting Information). Electronic absorption, λ_{max} (ϵ): in CH_3CN, 487 (674), 608 (1350) nm. Solution magnetic moment (298 K; MeCN): $\mu_{eff} = 1.83\ \mu_B$. E_{pc}(MeCN) = −990 mV vs SCE. Anal. Calcd for $FeC_{14}H_{30}Cl_3N_4OS_2Zn$: C, 29.9; H, 5.40; N, 9.97. Found: C, 29.5; H, 5.22; N, 9.93.

Protonation of $[Fe^{III}(ADIT)(ADIT\text{-}O)](Cl)\cdot MeCN$ (5b). Addition of 1.07 equiv of $HBF_4\cdot Et_2O$ (1.8 μL, 0.01 mmol) to **5b** (5.7 mg, 0.01 mmol) in MeCN at −40 °C causes a color change from grape-purple to cobalt-blue, and λ_{max} red-shifts from 575 to 622 nm in the electronic absorption spectrum. EPR (MeOH/EtOH glass (9:1), 7 K): $g_1 = 2.24$, $g_2 = 2.15$, $g_3 = 1.97$.

Protonation of $[Fe^{III}(ADIT)_2]Cl$ (3). Addition of 3.5 equiv of $HBF_4\cdot Et_2O$ (5.0 μL, 0.04 mmol) to **1** (4.2 mg, 0.01 mmol) in MeCN at −40 °C causes a color change from green to turquoise, and λ_{max} blue-shifts from 718 to 640 nm in the electronic absorption spectrum. EPR (MeCN/toluene glass (1:1), 7 K): $g_1 = 2.22$, $g_2 = 2.15$, $g_3 = 1.97$.

XAS Sample Preparation. All three model complexes, $Fe^{III}(ADIT)_2$ (**3**), $Fe^{III}(ADIT)(ADIT\text{-}O)$ (**5b**), and $Fe^{III}(ADIT)(ADIT\text{-}O\text{-}ZnCl_3)$ (**6**) were ground into a fine powder, dispersed as thinly as possible on sulfur-free Mylar tape in a dry, anaerobic glovebox (N_2) atmosphere, and mounted across the window of an aluminum plate. This procedure has been verified to minimize self-absorption effects. A 6.35 μm polypropylene film window protected the solid samples from exposure to air during transfer from the glovebox to the experimental sample chamber.

Data Collection and Reduction. XAS data were measured at the Stanford Synchrotron Radiation Laboratory using the 54-pole wiggler beam line 6-2. Details of the experimental configuration for low-energy studies have been described in an earlier publication.[46] The data reduction and error analysis follow the same method discussed in earlier publications except that, for pre-edge subtraction, the PYSPLINE program (written by A. Tenderholt, Stanford University) was used instead of the standard splining program in EXAFSPAK.[47]

Fitting Procedure. Pre-edge features were fit by pseudo-Voigt line shapes (sums of Lorentzian and Gaussian functions). This line shape is appropriate as the experimental features are expected to be a convolution of a Lorentzian transition envelope and a Gaussian line shape imposed by the spectrometer optics.[48,49] A fixed 1:1 ratio of Lorentzian to Gaussian contribution successfully reproduced the pre-edge features. The rising edge was also fit with pseudo-Voigt line shapes. Good fits reproduce the data and its second derivative using a minimum number of peaks. The intensity of a pre-edge feature (peak area) is the sum of the intensities of all the pseudo-Voigt peaks that successfully fit the feature in a given fit. The reported intensity values for the proteins are an average of all good pre-edge fits.

Computational Details. All calculations were performed on dual-CPU Pentium Xeon 2.8 GHz workstations using the Amsterdam Density Functional (ADF) program, version 2004.01, developed by Baerends et al.,[50,51] and with the Gaussian 03 package.[52] A triple-ζ Slater-type orbital basis set (ADF basis set TZP) with a single polarization function at the local density approximation of Vosko, Wilk, and Nusair,[53] with nonlocal gradient corrections described by Becke[54] and Perdew,[55] was

(41) Evans, D. A. *J. Chem. Soc.* **1959**, 2003−2005.
(42) Live, D. H.; Chan, S. I. *Anal. Chem.* **1970**, *42*, 791−792.
(43) Van Geet, A. L. *Anal. Chem.* **1968**, *40*, 2227−2229.
(44) Sandrinelli, F.; Perrio, S.; Beslin, P. *J. Org. Chem.* **1997**, *62*, 8626−8627.
(45) Shoner, S.; Barnhart, D.; Kovacs, J. A. *Inorg. Chem.* **1995**, *34*, 4517−4518.
(46) Hedman, B.; Frank, P.; Gheller, S. F.; Roe, A. L.; Newton, W. E.; Hodgson, K. O. *J. Am. Chem. Soc.* **1988**, *110*, 3798−3805.
(47) Shadle, S. E.; Hedman, B.; Hodgson, K. O.; Solomon, E. I. *Inorg. Chem.* **1994**, *33*, 4235−4244.
(48) Agarwal, B. K. *X-ray Spectroscopy*; Springer-Verlag: Berlin, 1979; p 276.
(49) Tyson, T. A.; Roe, A. L.; Frank, P.; Hodgson, K. O.; Hedman, B. *Phys. Rev. B* **1989**, *39A*, 6305−6315.
(50) Baerends, E. J.; Ellis, D. E.; Roos, P. *Chem. Phys.* **1973**, *2*, 41−51.
(51) te Velde, G.; Baerends, E. J. *Int. J. Comput. Phys.* **1992**, *99*, 84−98.
(52) Frisch, M. J.; et al. *Gaussian 03*, Revision C.02; Gaussian, Inc.: Wallingford, CT, 2004.
(53) Vosko, S. H.; Wilk, L.; Nusair, M. *Can. J. Phys.* **1980**, *58*, 1200−1211.
(54) Becke, A. D. *Phys. Rev. A: Gen. Phys.* **1988**, *38*, 3098−3100.
(55) Perdew, J. P. *Phys. Rev. B* **1986**, *33*, 8822−8224.

Table 1. Crystal Data for $[Fe^{III}(ADIT)(ADIT\text{-}O)](Cl)\cdot MeCN\cdot PhS(O)_2NH_2$ (**5a**) and $[Fe^{III}(ADIT)(ADIT\text{-}O\text{-}ZnCl_3)]$ (**6**)

	5a	6
formula	$C_{22}H_{40}ClFeN_6O_3S_3$	$C_{14}H_{30}FeN_4O\ Cl_3S_2Zn$
MW (g/mol)	624.08	562.11
temp (K)	130(2)	130(2)
unit cell[a]	monoclinic	orthorhombic
space group	$P2_1/c$	P_{bca}
a (Å)	13.5500(8)	15.4610(5)
b (Å)	9.9180(6)	14.4680(6)
c (Å)	25.0040(19)	20.5360(11)
α (°)	90	90
β (°)	117.413(2)	90
γ (°)	90	90
V (Å^3)	2982.9(3)	4593.7(3)
Z	4	8
σ_{calc} (mg/m^3)	1.390	1.626
R^b	0.0557	0.0466
R_w	0.0940	0.0600
GOF	0.999	1.001

[a] In all cases, Mo Kα ($\lambda = 0.71070$ Å) radiation. [b] $R = \sum||F_o| - |F_c||/\sum|F_o|$; $R_w = [\sum w(|F_o| - |F_c|)^2/\sum wF_o^2]^{1/2}$, where $w^{-1} = [\sigma^2_{count} + (0.05F^2)^2]/4F^2$.

employed. The molecular orbitals were plotted using Molden version 5.1 and gOpenmol version 2.2.

X-ray Crystallographic Structure Determination. A purple crystal plate, 0.48 × 0.19 × 0.05 mm, of **5a** was mounted on a glass capillary with epoxy. Data were collected at −143 °C. The crystal-to-detector distance was set to 30 mm, and exposure time was 70 s per degree for all data sets with a scan width of 1°. The data collection was 97.7% complete to 23.25° in θ. A total of 7755 partial and complete reflections were collected, covering the indices $h = -14$ to 15, $k = -9$ to 10, $l = -27$ to 27. Of those, 4170 reflections were symmetry independent, and the $R_{int} = 0.1133$ indicated that the data was fair. Indexing and unit cell refinements indicated a monoclinic P lattice in the space group $P2_1/c$ (No. 14).

A black prism, 0.24 × 0.15 × 0.10 mm, of **6** was submerged in mineral oil, placed on a glass capillary, and mounted over a stream of cold nitrogen gas (−143(2) °C). The crystal-to-detector distance was set to 30 mm, and exposure time was 20 s per degree for all data sets with a scan width of 1°. The data collection was 87.1% complete to 27.49° in θ. A total of 8692 reflections were collected, covering the indices $h = -19$ to 19, $k = -14$ to 14, $l = -26$ to 26. Of those, 4595 reflections were symmetry independent, and the $R_{int} = 0.1032$ indicated that the data was fair. Indexing and unit cell refinements indicated an orthorhombic P lattice in the space group P_{bca} (No. 61).

The data for both **5a** and **6** were integrated and scaled using Denzo-hkl-SCALEPACK, and an absorption correction was performed using SORTAV. Solution by direct methods (SIR97) produced a complete heavy-atom phasing model consistent with the proposed structures. All non-hydrogen atoms were refined anisotropically by full-matrix least-squares methods, while all hydrogen atoms were then located using a riding model. Crystal data for **5a** and **6** are presented in Table 1. Selected bond distances and angles are assembled in Table 2 (below).

Results and Discussion

Synthesis and Structure of Singly Oxygenated $[Fe^{III}(ADIT)(ADIT\text{-}O)]^+$ (5). The thiolate-ligated iron complex, $[Fe^{III}(ADIT)_2]^+$ (**3**), described by our group prior to the NHase crystal structure,[3] models the electronic and magnetic properties of the NHase non-heme iron site.[45,56] Like the NHase active site,[7,11] complex **3** is low-spin ($S = {}^1/_2$) over a wide temperature range, stabilized in the 3+ oxidation state ($E_{1/2} = -1.01$ V vs SCE), and intense green in color ($\lambda_{max} = 718$ (2500) nm). A low spin state is unexpected for non-heme iron, especially when ligated by π-donors such as RS^-, which tend to decrease 10Dq.[57] Addition of 1.4 equiv of *tert*-butyl *N*-sulfonyloxaziridine (**4**) to a MeOH solution of **3** causes the solution color to change from green to grape-purple, and results in the addition of a single oxygen atom to the coordination sphere, as determined by ESI-MS. The oxidant in this reaction, **4**, has been used previously to oxygenate free thiols.[44] The structure of the product of reaction 1, $[Fe^{III}(ADIT)(ADIT\text{-}O)]^+$ (**5**), was determined by

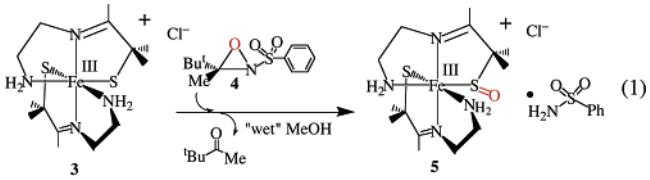

(1)

X-ray crystallography and found to contain a singly oxygenated thiolate sulfur (i.e., a sulfenate) coordinated to the metal ion. As shown in the ORTEP of Figure 2, the iron of $[Fe^{III}(ADIT)(ADIT\text{-}O)]^+$ (**5**) is six-coordinate and ligated by one thiolate sulfur (S(2)), two imine nitrogens (N(2) and N(4)), and two amine nitrogens (N(1) and N(3)), in addition to the singly oxygenated sulfenate sulfur (S(1)). Key bond distances and angles of mono-thiolate/sulfenate-ligated **5a** are compared with those of di-thiolate-ligated **3** in Table 2. The sulfenate Fe−S(1) bond length in **5a** is 0.052 Å longer than both of the Fe−S thiolate bonds in **3**, showing that the interaction between the metal and oxygenated sulfur weakens slightly as a result of oxygenation. The unmodified iron thiolate Fe−S(2) bond, on the other hand, is 0.038 Å shorter in **5a** relative to that in the parent unoxygenated compound **3**. The Fe−N(3) and Fe−N(4) distances in **5a** also shrink (by 0.04 and 0.02 Å, respectively) as a result of oxygen atom addition, consistent with an increase in Lewis acidity of the metal ion (Table 2). The unmodified thiolate Fe−S(2) bond is 0.086 Å shorter than the oxygenated

Table 2. Comparison of Selected Metrical Parameters for the Cations of $[Fe^{III}((ADIT)_2]Cl$ (**3**), $[Fe^{III}(ADIT)(ADIT\text{-}O)]Cl\cdot H_2NS(O)_2Ph\cdot MeCN$ (**5a**), and $[Fe^{III}(ADIT)(ADIT\text{-}OZnCl_3)]$ (**6**)[a]

	3	5a	6
Fe(1)−S(1)	2.200(1)	2.255(2)	2.255(1)
Fe(1)−S(2)	2.207(1)	2.169(2)	2.161(1)
Fe(1)−N(1)	2.043(3)	2.043(4)	2.029(3)
Fe(1)−N(2)	1.938(2)	1.931 (5)	1.945(4)
Fe(1)−N(3)	2.059(3)	2.019(4)	2.022(3)
Fe(1)−N(4)	1.938(2)	1.922(5)	1.938(3)
S(1)−O(1)		1.550(4)	1.565(3)
Zn−O(1)			1.978(3)
Zn−Cl(1)			2.223(1)
Zn−Cl(2)			2.289(1)
Zn−Cl(3)			2.255(1)
Fe−S(1)−O(1)		109.1(2)	105.8(1)
Fe−S(1)−C(4)	99.1(1)	97.6(2)	99.1(2)
O(1)−S(1)−C(4)		105.9(2)	102.3(2)
S(1)−O(1)−Zn			124.1(1)
S(1)−Fe−N(1)	167.9(1)	168.9(2)	168.1(1)
S(2)−Fe−N(3)	168.9(1)	170.9(2)	169.7(1)

[a] Bond lengths and bond angles are given in angstroms and degrees, respectively.

(56) Jackson, H. L.; Shoner, S. C.; Rittenberg, D.; Cowen, J. A.; Lovell, S.; Barnhart, D.; Kovacs, J. A. *Inorg. Chem.* **2001**, *40*, 1646−1653.

(57) Kennepohl, P.; Neese, F.; Schweitzer, D.; Jackson, H. L.; Kovacs, J. A.; Solomon, E. I. *Inorg. Chem.* **2005**, *44*, 1826−1836.

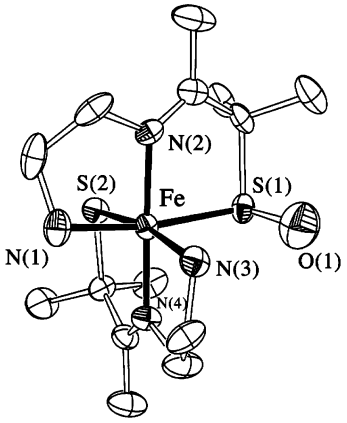

Figure 2. ORTEP diagram of the cation of $[Fe^{III}(ADIT)(ADIT\text{-}O)]Cl\cdot MeCN\cdot PhS(O)_2NH_2$ (**5a**), showing atom labeling scheme. All hydrogen atoms have been omitted for clarity.

sulfenate Fe−S(1) bond of **5a** (Table 2). This implies that the iron−thiolate Fe−S(2) bond becomes stronger as a result of single oxygen atom addition to the other sulfur S(1) (Figure 2).

Sulfur K-Edge X-ray Absorption Spectroscopy (XAS) and Density Functional Theory (DFT) Calculations. To understand the origin of the observed decrease in the unmodified Fe−S bond length (Fe−S(2)) resulting from oxygen atom addition to **3**, sulfur K-edge XAS data was obtained and DFT calculations were performed. S K-edge XAS allows one to directly probe the covalency of metal−thiolate (M−S) bonds and has proven useful in establishing how these properties contribute to the function of both metalloenzymes and model compounds.[25,58−65] Although the main feature at the sulfur K-edge is the sulfur 1s→4p transition, transitions between S_{1s} and any unoccupied orbital that has S_{3p} character, including the σ^*(C−S)and σ^*(Fe−S) (with e_g^* Fe_{3d} character), gain intensity, because the 1s→3p transition is also electric dipole allowed. The intensity of these transitions is directly proportional to the extent of S_{3p} mixing, as reflected by the covalency parameter (α^2) in eq 2,[66] where $I(S_{1s}\rightarrow Fe_{3d})$ is the intensity of the pre-

$$I(S_{1s}\rightarrow Fe_{3d}) = \alpha^2\langle S_{1s}|\mathbf{r}|S_{3p}\rangle \qquad (2)$$

edge feature, $\langle S_{1s}|\mathbf{r}|S_{3p}\rangle$ is the intensity of a pure ligand-based 1s→3p, transition which depends on the Z_{eff} of the sulfur atom, and α^2 is the covalency parameter as defined by $\Psi^* = (1-\alpha^2)^{1/2}|Fe_{3d}\rangle + \alpha|S_{3p}\rangle$. Since the co-crystallized benzenesulfonamide of **5a** complicated the S K-edge spectrum, a method of generating the sulfonamide-free derivative **5b** was developed

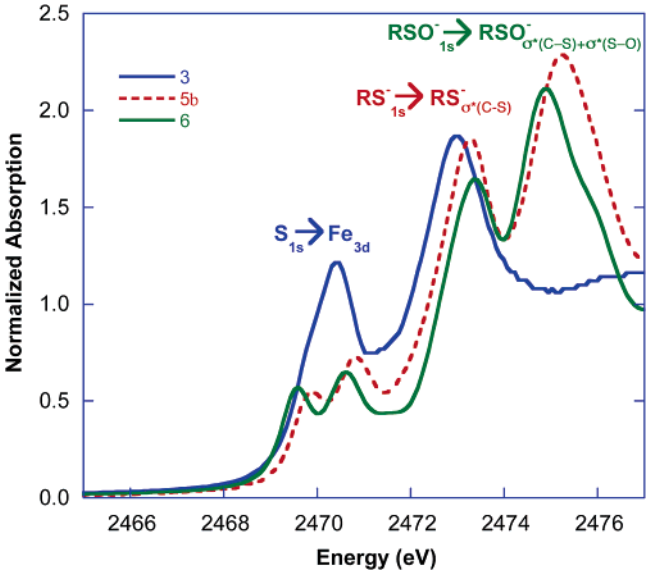

Figure 3. Sulfur K-edge XAS spectra for $[Fe^{III}(ADIT)_2]^+$ (**3**) (in blue), $[Fe^{III}(ADIT)(ADIT\text{-}O)]^+$ (**5b**) (in red), and $[Fe^{III}(ADIT)(ADIT\text{-}O\text{-}ZnCl_3)]$ (**6**) (in green).

(see Experimental section). As shown in Figure 3, the S K-edge XAS spectra for $[Fe^{III}(ADIT)_2]^+$ (**3**) and sulfonamide-free $[Fe^{III}$-$(ADIT)(ADIT\text{-}O)]^+$ (**5b**) contain three distinct transition envelopes — one between 2469 and 2471 eV, assigned to $S_{1s}\rightarrow Fe_{3d}$ *pre-edge* transitions (Table 3), one at 2473 eV, assigned to a thiolate (RS^-) $S_{1s}\rightarrow\sigma^*$(C−S) transition, and one at 2475 eV, assigned to sulfenate (RS-O^-) $S_{1s}\rightarrow\sigma^*$(C−S) and $S_{1s}\rightarrow\sigma^*$(S−O) transitions. The oxidized sulfenate $S_{1s}\rightarrow\sigma^*$(C−S) transition (at 2475 eV) is shifted 2 eV above that of the unmodified thiolate (RS_u^-) ligand, reflecting the stabilization of the RS-O^- ligand's S_{1s} orbital. For both **3** and **5b**, the unmodified thiolate's $S_{1s}\rightarrow Fe_{3d}$ *pre-edge region* consists of five transitions — one involving a $S_{1s}\rightarrow t_2$ (singly occupied dπ low-spin Fe(III) orbital) transition (β-spin) and four involving $S_{1s}\rightarrow e$ (empty dσ low-spin Fe(III) orbitals) transitions (α- and β-spin). The integrated intensities (*I*, Table 3) of the pre-edge thiolate $S_{1s}\rightarrow t_2$ transition increase from 0.35 in **3** to 0.47 in **5b**. This corresponds to two Fe−S thiolate bonds, each with 10.5% S_{3p} character in **3**, and one thiolate Fe−S_u bond (Figure 4), with 27% S_{3p} character in **5b**. From the integrated intensities of the e-feature, it is apparent that the σ-contribution to the iron thiolate bonding also increases from 30.5% per Fe−S bond in **3** to 45% per Fe−S_u bond in **5b**. This provides quantitative experimental evidence for an increase in the covalency of the thiolate Fe−S_u bond (Figure 4) upon oxygen atom addition to the other sulfur (S_m).

DFT calculations nicely reproduce the increase in the Fe−S_u bond covalency observed by S K-edge XAS, and the DFT-optimized distances and angles (Table 4) are in good agreement with the crystallographically determined metrical parameters (Table 2).[67] As shown in the MO diagram of Figure 5, the t_2 hole (singly occupied molecular orbital, SOMO) for **3** lies in the π^*(Fe−S) d_{xy} orbital and possesses 24% S_{3p} character (12% on each thiolate sulfur). The e set of σ^*(Fe−S) $d_{x^2-y^2}$ and d_{z^2} orbitals possess 28% and 6% S_{3p} character, respectively. The t_2 hole for **5** also lies in the d_{xy} orbital, which is predominantly

(58) Szilagyi, R. K.; Bryngelson, P. A.; Maroney, M. J.; Hedman, B.; Hodgson, K. O.; Solomon, E. I. *J. Am. Chem. Soc.* **2004**, *126*, 3018−3019.
(59) George, S. D.; Metz, M.; Szilagyi, R. K.; Wang, H.; Cramer, S. P.; Lu, Y.; Tolman, W. B.; Hedman, B.; Hodgson, K. O.; Solomon, E. I. *J. Am. Chem. Soc.* **2001**, *123*, 5757−5767.
(60) Szilagyi, R. K.; Lim, B. S.; Glaser, T.; Holm, R. H.; Hedman, B.; Hodgson, K. O.; Solomon, E. I. *J. Am. Chem. Soc.* **2003**, *125*, 9158−9169.
(61) Anxolabéhère-Mallart, E.; Glaser, T.; Frank, P.; Aliverti, A.; Zanetti, G.; Hedman, B.; Hodgson, K. O.; Solomon, E. I. *J. Am. Chem. Soc.* **2001**, *123*, 5444−5452.
(62) Dey, A.; Glaser, T.; Moura, J. J. G.; Holm, R. H.; Hedman, B.; Hodgson, K. O.; Solomon, E. I. *J. Am. Chem. Soc.* **2004**, *126*, 16868−16878.
(63) Glaser, T.; Bertini, I.; Moura, J. J. G.; Hedman, B.; Hodgson, K. O.; Solomon, E. I. *J. Am. Chem. Soc.* **2001**, *123*, 4859−4860.
(64) Solomon, E. I.; Hedman, B.; Hodgson, K. O.; Dey, A.; Szilagyi, R. K. *Coord. Chem. Rev.* **2005**, *249*, 97−129.
(65) Glaser, T.; Hedman, B.; Hodgson, K. O.; Solomon, E. I. *Acc. Chem. Res.* **2000**, *33*, 859−868.
(66) Neese, F.; Hedman, B.; Hodgson, K. O.; Solomon, E. I. *Inorg. Chem.* **1999**, *38*, 4854−4860.

(67) The Fe−N bonds are an exception, since they are longer (0.03−0.06 Å) than the crystallographically observed distances.

Table 3. Fitted Sulfur K-Edge XAS Pre-edge Positions and Intensities

	t_2			e						
	energy	*I*	% S_{3p}	energy	*I*	% S_{3p}	energy	*I*	% S_{3p}	total %S_{3p}
3	2469.9	0.35 ± 0.06	21 ± 6	2470.5	0.84 ± 0.06	50 ± 6	2471.4	0.16 ± 0.05	11 ± 5	61
5b	2469.8	0.47 ± 0.01	27 ± 1	2470.8	0.62 ± 0.01	36 ± 1	2471.6	0.15 ± 0.06	9 ± 5	45
6	2469.5	0.51 ± 0.01	30 ± 1	2470.5	0.57 ± 0.01	34 ± 2	2471.5	0.21 ± 0.03	12 ± 2	46

Table 4. DFT-Optimized Bond Lengths (Å) and Angles (deg)

	Fe–S_u	Fe–S_m	Fe–N_u	Fe–N_m	Fe–N_{ax}	C–S_u–Fe	C–S_m–Fe
$[Fe^{III}(ADIT)_2]^+$ (**3**)	2.21	2.21	2.14	2.14	1.95	98	98
$[Fe^{III}(ADIT)(ADIT\text{-}O)]^+$ (**5**)	2.19	2.31	2.06	2.13	1.93	99	95
$[Fe^{III}(ADIT)(ADIT\text{-}O\text{-}ZnCl_3)]$ (**6**)	2.20	2.29	2.05	2.12	1.94	99	96
$[Fe^{III}(ADIT)(ADIT\text{-}OH)]^{2+}$ (**5**-H^+)	2.19	2.27	2.08	2.06	1.94	99	100

π-antibonding with respect to the unmodified Fe−S_u bond (Figure 4) and possesses 23% S_{3p} character. The calculated increase in Fe−S_u bond covalency (from 12% per bond in **3** to 23% per bond in **5b**) upon oxygen atom addition is thus in good agreement with S K-edge data (from 10.5% per bond in **3** to 27% per bond in **5**; Table 3). Only one Fe−S bond is included in the total π-covalency of **5** because the modified RS-O^- fragment only interacts with the e-set of d orbitals and has no interaction with the d_{xy} π-orbital. This is because its π-symmetry orbital is involved in the S−O σ-bond (Figure 6). The Fe $d_{x^2-y^2}$ orbital of **5** is antibonding with respect the RS-O^- ligand and has significant contribution from the RS-O^- oxygen. This is because the S_{3p} orbital, which is involved in σ*-overlap with the Fe $d_{x^2-y^2}$, is also involved in π*-overlap with one of the O_{2p} orbitals (Figure 6). This S−O π-bond does not contribute to the S−O bond strength, since both the bonding (π) and antibonding (π*) orbitals are occupied. However the S−O π*-orbital has 50% S_{3p} character (Figure 6, HOMO) and thus can reasonably overlap in a σ-fashion with the metal $d_{x^2-y^2}$. The resulting MO represents the β LUMO of **5** shown in Figure 5. Although the S_{3p} coefficient of this donor orbital is less than that of a RS^- donor orbital, its π*-interaction with the O_{2p} elevates its energy relative to that of a RS^- donor orbital (by ~0.5 eV), favoring interaction with the Fe_{3d} orbital.

Overall, the %S_{3p} character and its energy distribution obtained from DFT calculations agree well with the experimental data, illustrating the compensatory role of the unmodified thiolate. The XAS data show, however, that the %S_{3p} character in the t_2 hole of **3** (10.5%) is in fact less than half of that for **5b** (27%) per thiolate Fe−S bond. This overcompensation by the unmodified thiolate is not reproduced in the DFT calculations, which is consistent with the fact that these calculations underestimate the shortening of the Fe−S bond (0.04 Å in X-ray vs 0.02 Å in DFT).

Changes to the Electronic Structure Upon Single Oxygen Atom Addition to $[Fe^{III}(ADIT)_2]^+$ (3). The dramatic color change (from green to grape-purple) associated with oxygen atom addition to **3** suggested that sulfur oxidation caused fairly major changes to the metal complex's electronic structure. Notable changes to the Fe−S bonding were detected by sulfur K-edge XAS and X-ray crystallography, and DFT calculations predicted this. Although π-interactions are lost between the oxygenated sulfur (S_m; Figure 4) and the metal ion, the unmodified thiolate (S_u) more than compensates for this by increasing its covalent bond strength. This is due in part to the fact that the oxygen shifts electron density away from the metal,

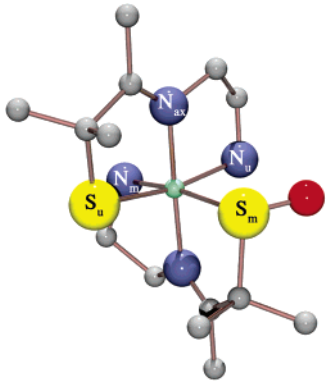

Figure 4. Schematic representation of $[Fe^{III}(ADIT)(ADIT\text{-}O)]^+$ (**5**), showing the modified (S_m) and unmodified (S_u) thiolates.

making it more Lewis acidic. Decreases in the Fe−N bond lengths observed in the X-ray crystal structure (Table 2) support this. One could conceivably determine the extent to which the shift in electron density toward the oxygen is offset by an increased π-back-donation from the unmodified thiolate sulfur (S_u; Figure 4) by examining the electronic absorption spectrum of **5** and comparing it with that of **3**. The electronic absorption spectra of dithiolate-ligated low-spin Fe^{III} complexes, such as **3**, have been shown to be dominated by an intense $\pi S \rightarrow Fe$ d_{xy} charge-transfer band.[57] If the metal ion Lewis acidity were to increase upon oxygen atom addition, then one would expect the $\pi S \rightarrow Fe$ d_{xy} transition to red-shift, since the metal ion orbitals would drop in energy toward the thiolate sulfur orbitals. The oxygenated sulfur would not contribute to the spectrum, since these orbitals would drop well below those of the metal ion. If the remaining thiolate donor RS_u^- were to back-donate exactly the same amount of electron density removed, then the $\pi S \rightarrow Fe$ d_{xy} CT band would not shift. If, on the other hand, the RS_u^- thiolate overcompensates by π-back-bonding more electron density than was removed, then the $\pi S \rightarrow Fe$ d_{xy} CT band would blue-shift. The electronic absorption spectrum in Figure 7 demonstrates that the latter occurs. The blue-shift caused by oxygen atom addition is similar in direction to that induced by H-bonding between the thiolates of **3** and protic solvents;[56] however, it is considerably larger in magnitude for oxygen atom addition (3463.7 cm^{-1} (9.9 kcal/mol) versus H-bonding (502.4 cm^{-1} (1.44 kcal/mol); Table 5).[56]

Redox and Magnetic Properties. On the basis of the S K-edge XAS, electronic absorption, and X-ray crystallographic data, which show that π-back-donation from the unmodified thiolate RS_u^- increases in response to oxygen atom addition,

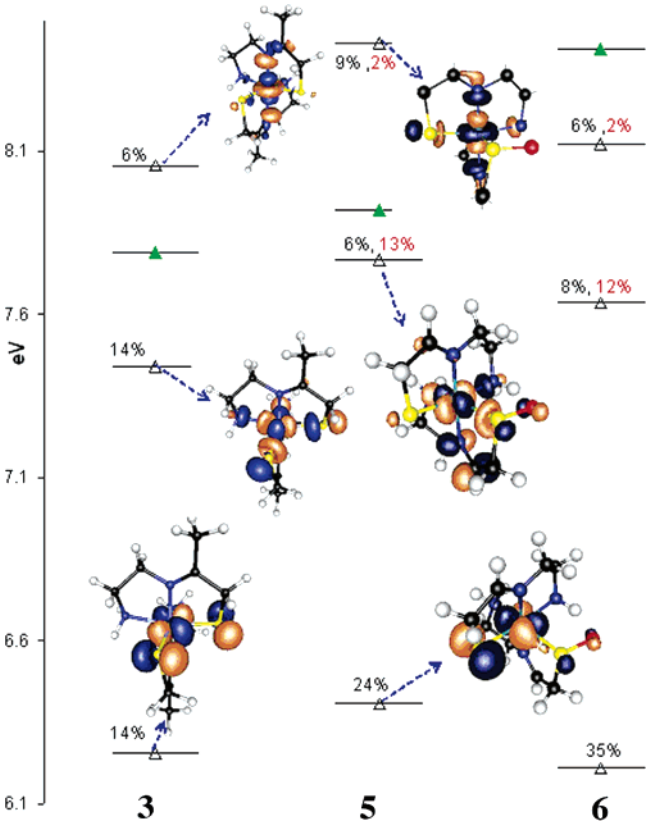

Figure 5. Energy level diagrams of **3**, **5**, and **6** (contours not shown). Only β unoccupied orbitals are shown. The $\%S_{3p}$ character per S atom is given next to the MOs. The green triangles represent low-lying unoccupied C=N π*-orbitals. The energies are referenced to the C−H bond energies of the CH_3 ligand substituent.

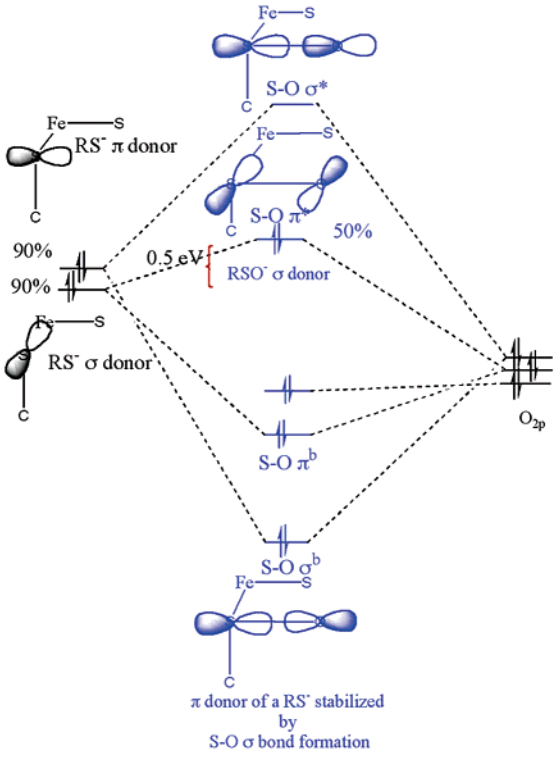

Figure 6. Schematic representation of the donor MOs of the oxidized RS-O$^-$ (in blue) and unmodified RS$^-$ (in black) ligands.

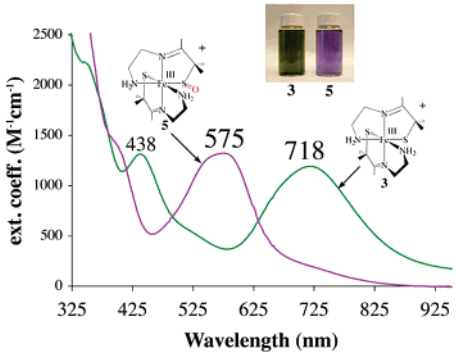

Figure 7. Comparison of the electronic absorption spectra of [Fe^{III}-$(ADIT)_2$]$^+$ (**3**) versus [Fe^{III}(ADIT)(ADIT-O)]$^+$ (**5a**) in MeCN solution at 298 K.

Table 5. Shift in the Lowest Energy LMCT Band Induced by Chemical Modification of Fe−SR or Fe−S(R)=O Bonds

chemical modification	LMCT shift direction	ΔE (LMCT transition) in cm^{-1}	ΔE (LMCT transition) in kcal/mol
O-atom addition to **3**	blue-shift	3464	9.91
H-bonding to **3**	blue-shift	502	1.44
H^+ addition to **3**	blue-shift	1697	4.85
H^+ addition to **5**	red-shift	1314	3.76
$ZnCl_2$ addition to **5**	red-shift	998	2.85

one would not expect the redox potential to shift dramatically. One would also expect the low-spin state to be maintained, given that the covalent Fe−S π-interaction increases upon oxygen atom addition. As shown by the redox potential obtained from the CV of Figure 8, the oxygenated sulfenate/thiolate ligand stabilizes iron in the 3+ oxidation state, as does the dithiolate ligand of **3** ($E_{1/2}$ = −1.01 vs SCE).[45,56] Although there is a slight cathodic shift upon oxygen atom addition, the magnitude of this shift (75 mV = 1.73 kcal/mol) is less than one might have anticipated, had there not been a second unmodified thiolate that compensates for the removal of electron density. In other words, the unmodified thiolate RS_u^- acts as an electronic buffer in maintaining a relatively constant Lewis acidity at the metal ion.

As shown by the inverse magnetic susceptibility versus temperature plot in Figure 9, **5b** obeys the Curie law and maintains the $S = {}^1/_2$ spin state (μ_{eff} = 1.88 μ_B) seen with **3** (μ_{eff} = 1.85 μ_B)[45] over the temperature range 5−300 K. The low-temperature (7 K) EPR spectrum of **5b** (Figure 10) also supports an $S = {}^1/_2$ ground-spin-state assignment. Dithiolate-ligated **3** displays a similar, albeit slightly less rhombic, EPR spectrum with g = 2.17, 2.11, 1.99. Thus, single oxygen atom addition to **3** does not significantly alter its magnetic properties.

Structural and Reactivity Properties of the Metal-Bound Sulfenate. Singly oxygenated sulfenates are typically unstable[68,69] unless coordinated to a transition metal.[27,39,68,70−74] DFT calculations described earlier indicated that the S−O bond of **5** is single and significantly polarized. This is supported by the X-ray structure. The S(1)−O(1) distance in **5a** (Table 2) falls at the long end of the reported range (1.510−1.551

(68) Allison, W. S. *Acc. Chem. Res.* **1976**, *9*, 293−299.

(69) Goto, K.; Holler, M.; Okazaki, R. *J. Am. Chem. Soc.* **1997**, *119*, 1460−1461.

(70) Grapperhaus, C. A.; Darensbourg, M. Y. *Acc. Chem. Res.* **1998**, *31*, 451−459.

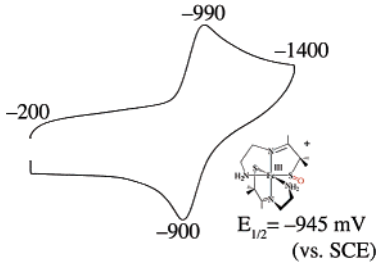

Figure 8. Cyclic voltammogram of $[Fe^{III}(ADIT)(ADIT\text{-}O)]^+$ (**5b**) in MeCN, with $Bu_4N(PF_6)$ supporting electrolyte (0.100 M), over the range from −200 to −1400 mV vs SCE.

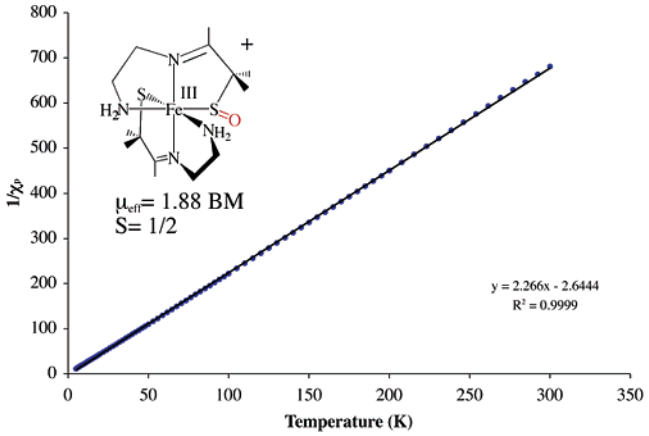

Figure 9. Inverse molar magnetic susceptibility $1/\chi_m$ vs temperature (T) plot for $[Fe^{III}(ADIT)(ADIT\text{-}O)]^+$ (**5b**) fit to an $S = {}^1/_2$ spin state.

Å),[39,70−74] and as shown by the angles about S(1), the coordinated sulfenate sulfur possesses trigonal pyramidal geometry. Although organic sulfenic acids are unstable, the S−OH bond in the few reported examples is significantly longer (range: 1.620−1.679 Å) than the S(1)−O(1) bond in **5a**, demonstrating that the Fe−S(R)−O$^-$ bond is less activated than a protonated RS−OH.[69,75,76]

Proton Addition. Addition of 1.07 equiv of HBF_4 to **5b** at −40 °C in MeCN (reaction 3) causes the color to change from grape-purple to cobalt-blue, and the $\pi S \rightarrow Fe\ d_{xy}$ CT band red-

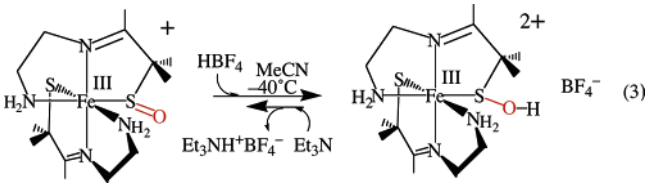

shifts by 47 nm (3.76 kcal/mol; Table 5) with very little loss of intensity (Figure 11). This spectral change is reversed upon the addition of 1.02 equiv of Et_3N (Figure S-3, Supporting Information). Warming to ambient temperature results in irreversible bleaching of color. The thermal instability of **5-H**$^+$ is consistent with the behavior of organic sulfenic acids.[69,77−79] The direction

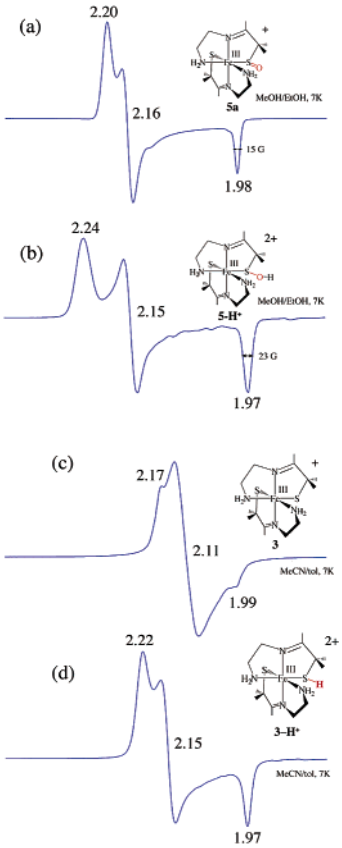

Figure 10. X-band EPR spectra of $[Fe^{III}(ADIT)(ADIT\text{-}O)]^+$ (**5a**) (a) versus protonated $[Fe^{III}(ADIT)(ADIT\text{-}OH)]^{2+}$ (b) in MeOH/EtOH glass at 7 K, and $[Fe^{III}(ADIT)_2]^+$ (**3**) (c) versus protonated $[Fe^{III}(ADIT)(ADIT\text{-}H)]^{2+}$ (d) in MeCN/toluene glass at 7 K.

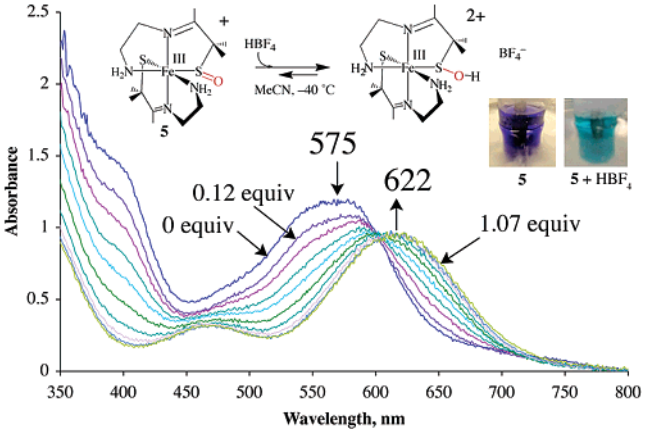

Figure 11. Electronic absorption spectrum showing the spectral changes which take place upon protonation of $[Fe^{III}(ADIT)(ADIT\text{-}O)]^+$ (**5**) with 1.07 equiv of HBF_4 (added in 0.12 aliquots) in MeCN at −40 °C.

of the shift induced by proton addition to **5** is opposite to that caused by oxygenation of **3**, and the magnitude is much less dramatic (Table 5). Given that the energy of the $\pi S \rightarrow Fe\ d_{xy}$ CT band was shown to reflect the Fe−S π-bond strength (vide supra), the relative energies of the CT band in **5-H**$^+$ versus **3** versus **5** (16 077 cm^{-1} (**5-H**$^+$) vs 13 928 cm^{-1} (**3**) vs 17 391 cm^{-1} (**5**)) imply that, although the thiolate Fe−S(2) π-bond of **5** weakens as a result of protonation, it remains stronger than it

(71) Adzamili, I. K.; Libson, K.; Lydon, J. D.; Elder, R. C.; Deutsch, E. *Inorg. Chem.* **1979**, *18*, 303−311.
(72) Buonomo, R. M.; Font, I.; Maguire, M. J.; Reibenspies, J. H.; Tuntulani, T.; Darensbourg, M. Y. *J. Am. Chem. Soc.* **1995**, *117*, 963−973.
(73) Font, I.; Buonomo, R.; Reibenspies, J. H.; Darensbourg, M. Y. *Inorg. Chem.* **1993**, *32*, 5897−5898.
(74) Cornman, C. R.; Stautler, T. C.; Boyle, P. D. *J. Am. Chem. Soc.* **1997**, *119*, 5986−5987.
(75) Ishii, A.; Komiya, K.; Nakayama, J. *J. Am. Chem. Soc.* **1996**, *118*, 12836−12837.
(76) Tripost, R.; Belaj, F.; Nachbaur, E. *Z. Naturforsch.* **1993**, *48b*, 1212−1222.
(77) Davis, F. A.; Billmers, R. L. *J. Org. Chem.* **1985**, *50*, 2593−2595.
(78) Bachi, M. D.; Gross, A. *J. Org. Chem.* **1982**, *47*, 897−898.
(79) Chou, T. S.; Burgtorf, J. R.; Ellis, A. L.; Lammert, S. R.; Kukolja, S. P. *J. Am. Chem. Soc.* **1974**, *96*, 1609−1610.

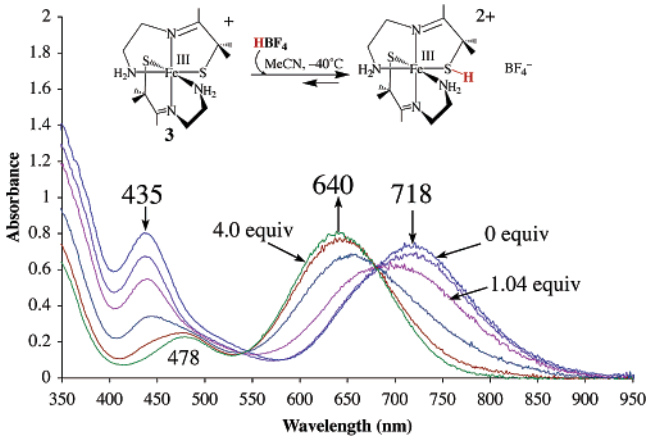

Figure 12. Electronic absorption spectrum showing the spectral changes which take place upon protonation of of $[Fe^{III}(ADIT)_2]^+$ (**3**) with 4.0 equiv of HBF_4 in MeCN at −40 °C.

was in dithiolate-ligated **3**. This would appear to rule out protonation at the unmodified thiolate sulfur. DFT calculations show that the unmodified Fe−S_u thiolate bond becomes even more covalent upon protonation of the RS-O^- oxygen (Figure 5) and that the $\%S_{3p}$ character increases from 54% in **5** to 63% in **5**-H^+. This suggests, as one would anticipate, that the RS-OH ligand is a poorer donor than a RS-O^-.

In contrast to the behavior of **5**, addition of HBF_4 to dithiolate-ligated $[Fe^{III}(ADIT)_2]^+$ (**3**) at −40 °C (reaction 4) causes the ligand-to-metal charge-transfer (LMCT) band to blue-shift (by 78 nm = 4.85 kcal/mol; Figure 12, Table 5), as opposed to red-shifting. The solution color changes from intense green to

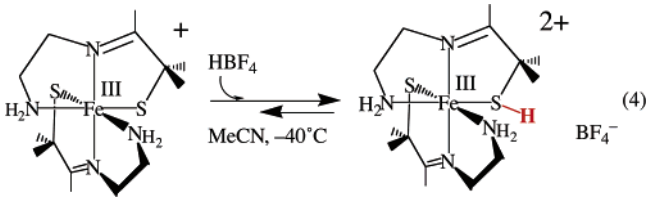

intense turquoise. The fact that the direction of this shift is opposite to that seen with **5** *implies that the protonation site is different* in **3** versus **5**. Strong acids (HCl, HBF_4) are required to protonate both **3** and **5**. Addition of weaker acids, such as HOAc, results in no reaction. More equivalents of HBF_4 are required to completely protonate **3** (4.0 equiv; as determined via a UV/vis monitored titration) versus **5** (1.1 equiv), however, suggesting that the protonation site in **3** is more acidic than that in **5**. Furthermore, protonated $[Fe^{III}(ADIT)(ADIT\text{-}H)]^{2+}$ (**3**-H^+) can only be generated in aprotic solvents at −40 °C (solution bleaching is observed in protic solvents), whereas protonated $[Fe^{III}(ADIT)(ADIT\text{-}OH)]^{2+}$ (**5**-H^+) is stable in both protic and aprotic solvents, as long as the temperature is below −40 °C. Again, this suggests that the protonation site is different in **3** versus **5**. As shown by the X-band EPR signal of Figure 10, the magnetic properties of **5** are not dramatically perturbed as a result of protonation, and the $S = {}^1/_2$ low-spin state is maintained. The signal does become slightly more rhombic (the g-spread, $\Delta g = g_{max} - g_{min}$, increases from 0.22 to 0.27), however, indicating that the coordination sphere has been subtly altered. ENDOR studies aimed at locating this proton are underway.[80] X-ray absorption spectroscopic (XAS) data are most

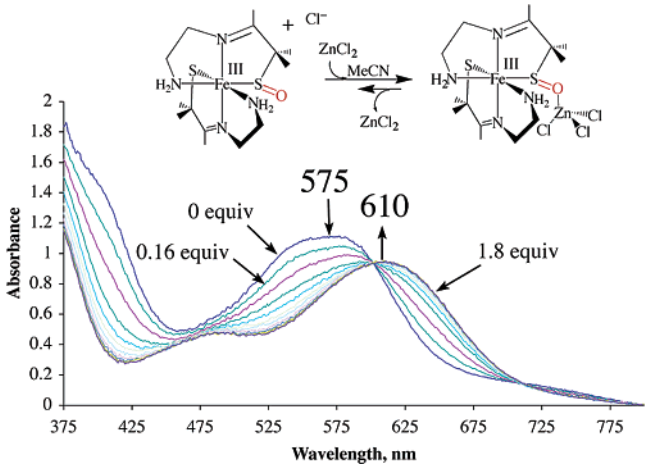

Figure 13. Electronic absorption spectrum showing the spectral changes which take place upon the addition of 1.8 equiv of $ZnCl_2$ to $[Fe^{III}(ADIT)(ADIT\text{-}O)]Cl$ (**5**) in MeCN at 25 °C.

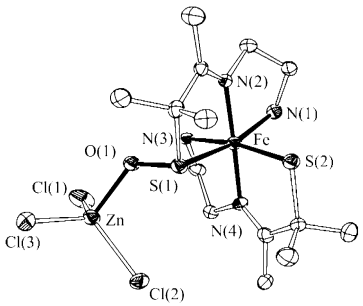

Figure 14. ORTEP diagram of $[Fe^{III}(ADIT)(ADIT\text{-}O\text{-}ZnCl_3)]$ (**6**), showing the atom labeling scheme. All hydrogen atoms have been omitted for clarity.

consistent with proton addition to the oxygen of **5**, as opposed to one of the nitrogens or sulfurs.[81]

Addition of Lewis Acidic $ZnCl_2$. Since protonated $[Fe^{III}(ADIT)(ADIT\text{-}OH)]^{2+}$ (**5**-H^+) is thermally unstable and could not be isolated, we decided to probe the reactivity of $[Fe^{III}(ADIT)(ADIT\text{-}O)]^+$ (**5**) with Lewis acids more likely to afford a stable derivative. Addition of 1.8 equiv of $ZnCl_2$ to $[Fe^{III}(ADIT)(ADIT\text{-}O)]Cl$ in MeCN causes the solution color to change from grape-purple to midnight-blue and the LMCT band to red-shift from 575 to 610 nm (Figure 13, Table 5). The direction of this shift is identical to that observed upon proton addition to **5**, but the magnitude of this shift is smaller (1314.1 cm^{-1} for H^+ vs 997.9 cm^{-1} for $ZnCl_2$). The product of this reaction, $[Fe^{III}(ADIT)(ADIT\text{-}O\text{-}ZnCl_3)]$ (**6**), is stable at ambient temperature and crystallized readily from MeCN (Figure 14). The sulfur K-edge XAS spectrum of **6** (Figure 3) shows an unmodified thiolate $S_{1s} \rightarrow t_2$ pre-edge transition at 2469.5 eV, the integrated intensity of which is consistent with a slight increase in the π-covalency of the Fe−S_u bond (from 27% to 30% S_{3p} character; Table 3) upon the addition of an electrophile to the sulfenate oxygen. DFT calculations replicate this increased covalency (Figure 5).

As shown in the ORTEP diagram (Figure 14), the Lewis acidic Zn^{2+} ion coordinates to the sulfenate oxygen of **6**. This lends support to the possibility that protons add to the sulfenate oxygen as well, although the steric requirements for $ZnCl_3^-$

(80) McNaughton, R.; Lugo-Mas, P.; Kovacs, J. A.; Hoffman, B., manuscript in preparation.
(81) Slonkina, E.; Dey, A.; Lugo-Mas, P.; Kovacs, J. A.; Solomon, E. I.; Hodgson, K. O.; Hedman, B., manuscript in preparation.

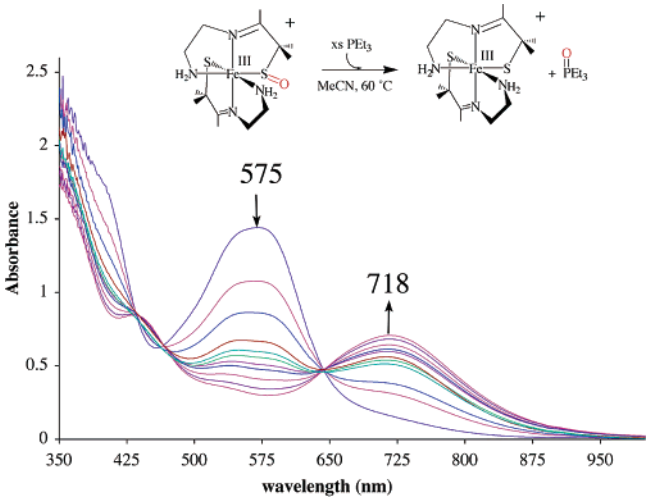

Figure 15. Electronic absorption spectrum, showing that PEt_3 (100 equiv; 220 mL of a 1 M solution in THF)) reacts with $[Fe^{III}(ADIT)(ADIT\text{-}O)]^+$ (**5**) in MeCN at 60 °C, over the course of 12 h, to afford $[Fe^{III}(ADIT)_2]^+$ (**3**).

might preclude binding to the inner coordination sphere N- or S-atoms. The Cl^- counterion present in **5a** binds to the Zn^{2+} ion of **6** to complete its tetrahedral coordination sphere. Zinc ($ZnCl_3^-$) binding does not noticeably affect the Fe−S(1) or Fe−S(2) bond lengths; however, it does slightly activate the S−O bond, as indicated by its slightly longer bond length (Table 2) and lower $\nu_{S=O}$ stretching frequency (893 cm^{-1} (Figure S-2, Supporting Information) in **6** vs 930 cm^{-1} in **5b**). As expected, the magnetic properties are not perturbed by Zn^{2+} ion addition, and the $S = {}^1/_2$ spin state is maintained (Figure S-5, Supporting Information). $ZnCl_2$ addition to $[Fe^{III}(ADIT)(ADIT\text{-}O)]^+$ (**5**) is reversible and highly solvent-dependent. In MeCN, the equilibrium favors neutral $[Fe^{III}(ADIT)(ADIT\text{-}O\text{-}ZnCl_3)]$ (**6**), and only 1.8 equiv of $ZnCl_2$ is required for complete conversion. In MeOH, on the other hand, the equilibrium favors monocationic $[Fe^{III}(ADIT)(ADIT\text{-}O)]^+$ (**5**), and 400 equiv of $ZnCl_2$ is required to completely convert **5** to **6**. Dissolution of crystalline samples of **6**, pre-isolated from MeCN, into either H_2O or MeOH results in its complete conversion to **5**.

Oxygen Atom Abstraction. The oxygen atom of **5** can be removed, albeit under forcing conditions, via the addition of PEt_3 at elevated temperatures. This reaction was monitored by electronic absorption spectroscopy, where $[Fe^{III}(ADIT)(ADIT\text{-}O)]^+$ (**5**) was shown to convert to $[Fe^{III}(ADIT)_2]^+$ (**3**) upon the addition of PEt_3, as shown in Figure 15. Triethylphosphine oxide ($Et_3P{=}O$) is detected in this reaction by mass spectrometry. The reactive nature of the coordinated sulfenate in **5** fits with the established reactivity patterns of organic sulfenates.[27,68,69] Sulfenates are particularly reactive and prone to both electrophilic and nucleophilic attack.[82,83] The slow reaction times and harsh conditions required to abstract the oxygen atom from **5** demonstrate, however, that once coordinated to Fe^{3+}, the sulfenate is less reactive.

Sulfenate-ligated **5** does not appear to react with nitriles (MeCN, isobutyronitrile), even at elevated temperatures and/or extreme pH conditions. Although this is not surprising, given

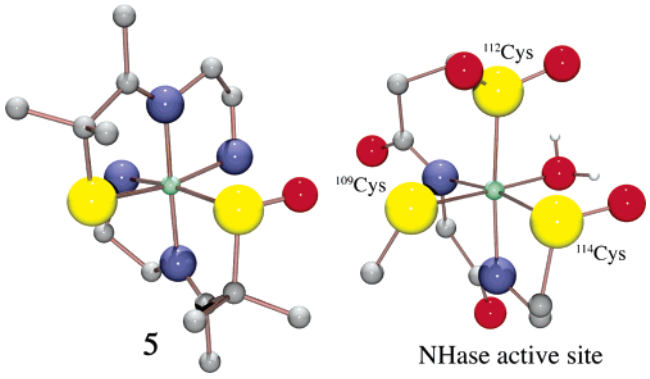

Figure 16. Comparison of the iron coordination environment of **5** with that of the NHase active site.

that the metal ion is coordinatively saturated, it has been suggested, on the basis of the demonstrated nitrile hydrolysis chemistry promoted by six-coordinate, sulfenate-ligated $[Co^{III}(L\text{-}N_2SOSO)(t\text{BuNC})_2]^-$, that nitrile hydrolysis occurs at the NHase sulfenate sulfur as opposed to the metal.[38] The analogous doubly oxygenated sulfinate derivative, $[Co^{III}(L\text{-}N_2SO_2SO_2)(t\text{BuNC})_2]^-$, does not hydrolyze nitriles,[38] again suggesting that reactivity is due to the specific properties of the singly oxygenated sulfenate.

Implications Regarding NHase Function. The results herein demonstrate that the unoxidized thiolate ligand plays the role of an "electronic buffer" in a series of model complexes, each of which contains at least one unmodified (i.e., unoxidized, deprotonated) thiolate ligand. The covalency of the $Fe-S_u$ bond increases as the other thiolate (S_m) becomes a poorer donor upon oxidation and electrophile addition. DFT calculations reproduce this compensating effect and also show that this effect originates from the fact that both thiolates compete for the same unoccupied or partially occupied 3d orbitals on the metal. Thus, it seems that the modification of one thiolate donor is an efficient way to control the interaction between the metal ion and the other thiolate donor. As shown in Figure 16, the topology of **5** (left) matches that of the NHase active site (right) in that it has one unmodified RS^- donor and one RS-O(H) donor in the same plane as those derived from ^{109}Cys and ^{114}Cys. In addition, both sites contain a set of two strong $N-\sigma$ donors. In contrast to the complexes studied here, however, the NHase unmodified thiolate (^{109}Cys) is positioned trans relative to the exchangeable sixth coordination site. On the basis of the results described herein, it seems likely that the oxidation/protonation/H-bonding state of the iron-bound cysteine sulfenic acid provides a mechanism for tuning the donor strength of the unmodified thiolate, which in turn would affect the pK_a, and lability of a trans-bound H_2O.

Summary and Conclusions. In summary, the synthesis and structure of the first oxidized sulfenate (RS-O^-)-ligated iron complex are described. Its redox, electronic, magnetic, reactivity, and bonding properties were examined and compared with those of its reduced dithiolate precursor. The unmodified thiolate ligand (RS_u^-) was shown to overcompensate for the lost $Fe-S_m$ π-bonding and shift in electron density toward the added oxygen atom by increasing its π-back-donation to the metal and forming a stronger covalent $Fe-S_u$ bond. In other words, the unmodified thiolate ligand acts as a buffer in modulating the electron density at the metal ion. This electronic buffering effect maintains a relatively constant redox potential, stabilizing iron in the 3+ oxidation state, even in the presence of an oxidized sulfenate ligand. With a hydrolytic metalloenzyme such as

(82) Sandrinelli, F.; Perrio, S.; Averbuch-Pouchot, M.-T. *Org. Lett* **2002**, *4*, 3619−3622.
(83) Farmer, P. J.; Verpeaux, J.-N.; Amatore, C.; Darensbourg, M. Y.; Musie, G. *J. Am. Chem. Soc.* **1994**, *116*, 9355−9356.

NHase, this would be important to avoid radical damage caused by O_2-induced Fenton chemistry. The unmodified cysteinate appears to play a *protective role* in that it prevents a potentially redox-active metal ion from attaining a potentially damaging (Fe^{2+}) oxidation state. It is also possible that the unmodified cysteinate plays a role in modulating the pK_a, lability, and nucleophilicity of the trans H_2O via its compensatory response to changes in the protonation state of the sulfenate ($RS\text{-}O^-$) oxygen.

Acknowledgment. This research was supported by NIH Grants GM45881 (J.A.K.), NIH-GM 40392 (E.I.S.), and RR-01209 (K.O.H.). SSRL operations are supported by the Department of Energy, Office of Basic Energy Sciences. The SSRL Structural Molecular Biology Program is supported by the National Institutes of Health, National Center for Research Resources, Biomedical Technology Program, and the Department of Energy, Office of Biological and Environmental Research. P.L.-M. gratefully acknowledges support by an NIH pre-doctoral minority fellowship (F31 GM73583-01). We thank Daniel Gamelin for helpful discussion, and Dan Patel, Nick Norberg, Jim Roe, and Terry Kitagawa for experimental assistance.

Supporting Information Available: Crystallographic data, in CIF format, for **5a** and **6**; IR spectra of [Fe^{III}(ADIT)(ADIT-O)](Cl)·MeCN (**5b**) and [Fe^{III}(ADIT)(ADIT-O-$ZnCl_3$)] (**6**), magnetic data for **6**, titration monitored by UV/vis, showing that $[Fe^{III}(ADIT)(ADIT\text{-}OH)]^{2+}$ can be reversibly deprotonated, all optimized coordinates and MO diagram of (ADIT-OH) ligand systems, and the complete ref 52. This material is available free of charge via the Internet at http://pubs.acs.org.

JA062706K